On the similarity of hillslope hydrologic function: a clustering approach based on groundwater changes

Fadji Z. Maina[1,2*], Haruko M. Wainwright[1], Peter James Dennedy-Frank[1], Erica R. Siirila-Woodburn[1]

[1] Energy Geosciences Division, Lawrence Berkeley National Laboratory 1 Cyclotron Road, M.S. 74R-316C, Berkeley, CA 94704, USA

[2]now at NASA Goddard Space Flight Center, Hydrological Sciences Laboratory, 8800 Greenbelt Rd, Greenbelt, 20771, MD, USA

*Corresponding Author: fadjizaouna.maina@nasa.gov

Abstract

Hillslope similarity is an active topic in hydrology because of its importance to improve our understanding of hydrologic processes and enable comparisons and paired studies. In this study, we propose a holistic bottom-up hillslope clustering based on a region's integrative hydrodynamic response quantified by the seasonal changes in groundwater levels ΔP. The main advantage of the ΔP clustering is its ability to capture recharge and discharge processes. We test the performance of the ΔP clustering by comparing it to seven other common hillslope clustering approaches. These include clustering approaches based on the aridity index, topographic wetness index, elevation, land cover, and machine-learning that jointly integrate multiple data. We assess the ability of these clustering approaches to identify and categorize hillslopes with similar static characteristics, hydroclimate, land surface processes, and subsurface dynamics in a mountainous watershed, the East River, located in the headwaters of the Upper Colorado River Basin. The ΔP clustering performs very well in identifying hillslopes with 6 out of the 9 characteristics studied. The variability among clusters as quantified by the coefficient of variation (0.2) is less in the ΔP and the machine learning approaches than in the others (>0.3 for TWI, elevation, and land cover). We further demonstrate the robustness of the ΔP clustering by testing its ability to predict hillslope responses to wet and dry hydrologic conditions, of which it performs well when based on average conditions.

Keywords: Hillslope, similarity, seasonal groundwater variations, integrated hydrologic modeling, hillslope clustering, hydrologic function

1. Introduction

The ability to delineate areas into spatially defined regions for their use in characterizing hydrologic flow and transport behavior is important for several reasons, including the assessment, monitoring, and modeling of water quantity and quality. Hillslopes are the scale at which hydrologic flow and transport processes can be tractably and frequently measured. It is also the scale at which flow and travel time are quantified, and the instrumentation, conceptualization, and modeling of hydrologic processes occur (Fan et al., 2019, Wainwright et al., 2022). While advancements have been made in the general understanding of hillslope dynamics over the last several decades, there is yet to be a globally agreed-upon classification and/or clustering for this important scale of interest in hydrology (McDonnell & Woods, 2004). Hydrologic signatures within hillslopes are the results of several simultaneous and nonlinear above- and below-ground processes. The uniqueness of a given location's characteristics (for example, the topography, geology, vegetation, etc.) limits our ability to draw general hypotheses and to develop a similarity framework (Beven, 2000). Nevertheless, a classification is needed to provide guidance on catchments and hillslopes comparisons (McDonnell & Woods, 2004), paired studies (Andréassian et al., 2012; Bosch & Hewlett, 1982; Brown et al., 2005), and improve our understanding of the changes in hydrologic processes across the world. Further, hillslope similarity is potentially an important step toward developing reduced-order models and machine learning algorithms, where identifying regions based on their similarities can substantially reduce computational costs (Chaney et al., 2018). The scaling of hillslope to catchment classifications can also be useful in the prediction of hydrologic behavior in ungauged basins (Sivapalan et al., 2003), an exceedingly important challenge.

Hillslope similarity clustering approaches include the Topographic Wetness Index TWI (Beven & Kirby, 1979), which was proposed to quantify the topographic control on hydrology as

topography plays a key role in the movement of water. Many other variants of this index have been later proposed to improve the definition of topographic similarity (Grabs et al., 2009; Hjerdt et al., 2004; Loritz et al., 2019). Other clustering approaches are based on hydroclimate (Carrillo et al., 2011), soil type and texture (Bormann, 2010), and land cover type (e.g., forest, urban, etc. (Wagener et al., 2007)). These indices assume that hillslopes with similar topography and land cover will have similar hydrologic responses. However, given that hydrologic processes are governed by many characteristics of the hillslope, clustering approaches relying on multiple landscape characteristics have also been proposed (Aryal et al., 2002; Sawicz et al., 2011). These top-down clustering approaches assume that areas with similar physical characteristics will lead to similar hydrologic processes (Oudin et al., 2010). Other clustering approaches use a bottom-up approach, where similarity is based on the hydrologic process. This clustering allows the estimation of the "hidden" hillslope characteristics such as soil texture, and geology that may drive similar hydrologic responses (Carrillo et al., 2011). Among the process-based clustering approaches existing in the literature we can cite: the Péclet number characterizing the diffusive and advective transfer of water at hillslope scale (Berne et al., 2005; S. W. Lyon & Troch, 2007; Steve W. Lyon & Troch, 2010) and the catchment seasonal water balance (Berghuijs et al., 2014). Other authors have derived hillslope similarities from subsurface flow dynamics (Harman & Sivapalan, 2009).

One challenge in developing a similarity framework is the inherent heterogeneity of a given hillslope. For example, Snow Water Equivalent (SWE), infiltration (I) and actual evapotranspiration (ET) distributions can range over an order of magnitude within a single hillslope (Wainwright et al., 2022). Defining a single integrative measure that can capture this spatio-temporal variability is difficult. However, groundwater fluctuations are often tightly linked

to seasonal changes in climate and have been shown to play an important role in surficial processes such as ET (Maina et al., 2022; Maina & Siirila-Woodburn, 2020; Maxwell & Condon, 2016). Thus, groundwater measures may serve as a good proxy for the aggregated hydrologic response. Groundwater dynamics could help overcome the issue of uniqueness of place because even if there are strong differences in the characteristics of the hillslope, the integrated response may be similar as some of the processes might not be important. Finally, the implications of groundwater changes are also important. For example, many regions are characterized by groundwater-dependent ecosystems or are hypothesized to have water table fluctuations affecting bedrock weathering rates and therefore the concentration and fluxes of metals and nutrients exports (e.g., Winnick et al., 2017).

In this study, we define a holistic bottom-up hillslope clustering using the integrative hydrologic response quantified by the seasonal changes in groundwater levels. A caveat to this clustering is that groundwater dynamics are difficult to quantify, and their measurements are frequently scarce. Hence, there are very few studies that use this variable to develop a hillslope similarity classification (Aryal et al., 2002; S. W. Lyon & Troch, 2007). However, today, thanks to advances in integrated hydrologic modeling (Brunner & Simmons, 2012; Maxwell & Miller, 2005), accurate quantification of the groundwater dynamics at high resolution in both time and space, as well as their interaction with the key land surface processes and features, is now feasible. These models (e.g., HydroGeoSphere (Brunner and Simmons, 2012), ParFlow (Maxwell & Miller, 2005), Advanced Terrestrial Simulator, (Coon et al., 2016)) that can be constrained with ground observations and measurements at ultra-high resolutions through aerial or remote sensing (i.e., drones, planes, or satellites) account for the two-way interactions between groundwater and land surface processes. Spatially resolved hydrologic flow models also enable us to jointly quantify

other hydrologic variables useful to identify hillslope with similar hydrologic responses, namely trends in ET, SWE, and I. Nevertheless, we acknowledge that groundwater dynamics in some regions such as arid areas could be disconnected to land surface processes and less dependent to many key physical features of the hillslope, which may impede the ability of the proposed clustering in these regions.

We test the proposed hillslope clustering on the site of the Department of Energy's (DOE) Watershed Function Scientific Focus Area (SFA) located in the headwaters of the Upper Colorado River Basin. The East River watershed is not only representative of many headwater catchments in the western United States in terms of its spatial heterogeneity of above and below-ground characteristics but also serves as an important proxy of water quantity and quality trends which ultimately impact a large population of water supply in the western United States for municipal, agriculture, and industrial use (Hubbard et al., 2018). We test the robustness of the proposed hillslope clustering by comparing it to seven other common hillslope clustering approaches based on the aridity index (AI), TWI, elevation, land cover and machine-learning approaches that jointly integrate multiple input data layers such as elevation, land cover, and geology, and model outputs including ET, and SWE. We assess the ability of these clustering approaches to identify and categorize hillslopes with similar physical characteristics (land cover and elevation), hydroclimate (precipitation and temperature), land surface processes (ET and SWE), subsurface dynamics (soil saturation, water table depth WTD, and seasonal changes in groundwater). We aim to provide answers to the following questions:

- What are the best clustering approaches for identifying hillslopes with similar hydrologic processes?

- Is a similarity index based on the seasonal groundwater variations sufficient to capture all the complex processes taking place at a hillslope scale?

2. Methodology

2.1. Modeling framework

2.1.1. Selected integrated hydrologic model: ParFlow-CLM

We use the integrated hydrologic model, ParFlow, which has the advantages of simulating the water and energy balance from the bedrock to the lower atmosphere and therefore connect groundwater dynamics with land surface processes. ParFlow solves the subsurface flow using the three-dimensional mixed form of the Richards equation (Richards, 1931) given by the following equation:

$$S_S S_W(\psi_P)\frac{\partial \psi_P}{\partial t} + \phi\frac{\partial S_W(\psi_P)}{\partial t} = \nabla.[K(x)k_r(\psi_P)\nabla(\psi_P - z)] + q_s \quad (1)$$

Where is S_S the specific storage [L^{-1}], $S_W(\psi_P)$ is the degree of saturation [-] associated with the subsurface pressure head ψ_P [L], t is the time [T], ϕ is the porosity [-], k_r is the relative permeability [-], z is the depth [L], q_s is the source/sink term [T^{-1}] and $K(x)$ is the saturated hydraulic conductivity [L T^{-1}] which is assumed to be a diagonal tensor with entries given as: $k_x(x)$, $k_y(x)$ and $k_z(x)$. We assumed in this work that the domain is isotropic, and that the tensor is equal to 1 for all the three directions at each cell of the discretized model. In the unsaturated zone, both S_W and k_r depend on the ψ. The relationships between S_W and k_r and ψ are described by the van Genuchten model (van Genuchten, 1980).

Overland flow (equation 2) is solved by the kinematic wave equation in two dimensions.

$$-k(x)k_r(\psi_0)\nabla(\psi_0 - z) = \frac{\partial \|\psi_0,0\|}{\partial t} - \nabla.\vec{v}\|\psi_0,0\| - q_r(x) \quad (2)$$

Where ψ_0 is the ponding depth, $\|\psi_0,0\|$ indicates the greater term between ψ_0 and 0, $\vec{v}$ is the depth averaged velocity vector of surface runoff [L T^{-1}], q_r is a source/sink term representing

147 rainfall and evaporative fluxes [L T^{-1}]. Surface water velocity at the surface in *x* and *y* directions,
148 (v_x) and (v_y) respectively, is computed using the following set of equations:

149 $$v_x = \frac{\sqrt{S_{f,x}}}{m}\psi_0^{\frac{2}{3}} \text{ and } \quad v_y = \frac{\sqrt{S_{f,y}}}{m}\psi_0^{\frac{2}{3}} \tag{3}$$

150 Where $S_{f,x}$ and $S_{f,y}$ friction slopes along *x* and *y* respectively and m is the manning's coefficient.
151 ParFlow employs a cell-centered finite difference scheme along with an implicit backward Euler
152 scheme and the Newton Krylow linearization method to solve these nonlinear equations. The
153 computational grid follows the terrain to mimic the slope of the domain (Maxwell, 2013).

154 ParFlow is coupled to the Community Land Model (CLM, (Dai et al., 2003)) which allows
155 for the simulation of important land surface processes such as ET and SWE and the quantification
156 of water leaving or entering the surface and subsurface (q_s and q_r respectively in the Richards and
157 kinematic wave equations). CLM models the thermal processes by closing the energy balance at
158 the land surface given by:

159 $$R_n(\theta) = LE(\theta) + H(\theta) + G(\theta) \tag{4}$$

160 Where $R_n$is the net radiation at the land surface [E/LT] a balance between the shortwave
161 and longwave radiation, LE is the latent heat flux [E/LT] which captures the energy required to
162 change the phase of water to or from vapor, *H* is the sensible heat flux [E/LT] and *G* is the ground
163 heat flux [E/LT]. All terms are a function of θ, the water content, which is computed by ParFlow.

164 Computing the different components of the energy balance requires meteorological
165 forcing, vegetative parameters, and soil moisture. The latter is computed by ParFlow using
166 equations 1 and 2. Meteorological forcing includes precipitation, temperature, east to west and
167 north to south wind speed, longwave and shortwave solar radiation, air pressure, and relative
168 humidity. Vegetative parameters include maximum and minimum leaf area index, stem area index,
169 aerodynamic roughness height, optical properties, stomatal physiology, roughness length, and

displacement height. More details about the coupling between ParFlow and CLM as well as the equations governing the snow dynamics and *ET* can be found in the following papers: Jefferson et al., (2015); Maxwell & Miller, (2005); Ryken et al., (2020). ParFlow-CLM has been used in many studies to understand the interactions between groundwater dynamics and lower atmosphere (Maina et al., 2022; Maina and Siirila-Woodburn, 2020) at different scales from watershed (Foster and Maxwell, 2019; Maina et al., 2020) to continental scale (Maxwell and Condon, 2016).

2.1.2. East River watershed model set-up

The East River watershed (Figure 1), located in the Upper Colorado Basin, is one of the two major tributaries that form the Gunnison River, which in turn accounts for just under half of the Colorado River's discharge at the Colorado-Utah border. The total area of this watershed is approximately 255 km^2 and the elevation varies from approximately 2700 to 3900 m. The watershed is characterized by strong heterogeneities in vegetation, geomorphology, and bedrock composition (Hubbard et al., 2018). The vegetation includes grasses, conifers, mixed conifers, aspens, and meadows and lies on a complex geologic terrain, which is comprised of a diverse collection of Paleozoic and Mesozoic sedimentary and unconsolidated rocks. The watershed is also characterized by a strong hydroclimate gradient. The average precipitation is 1200 mm/year while the average temperature is around 0°C. Because of its very low cold winter with temperature below 0°C, most of the winter precipitation is in the form of snow.

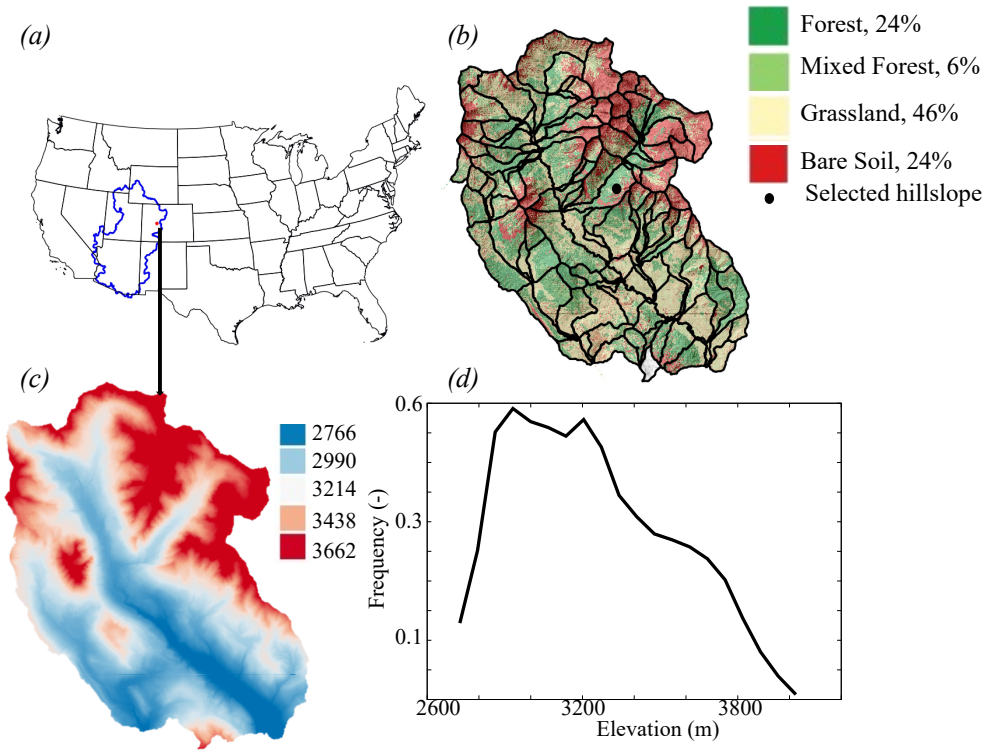

Figure 1: (a) location of the East River watershed, (b) land cover (NEON dataset, 2020), (c) LiDAR Digital elevation, and (d) elevation distribution within the East River.

ParFlow-CLM used here is based on a previous version of the East River watershed model, as described by Foster and Maxwell (2019). 5 layers constitute the model in the vertical direction with varying thickness from 0.1 m at the land surface to 21 m at the bottom of the domain. The land use and land cover are derived from the high-resolution airborne remote sensing NEON campaign (Chadwick, et al., 2020; Falco, et al., 2019; Goutlten, et al., 2020). From the hyperspectral spectrometer and LiDAR readings, 4 major types of land cover are grouped as follows: forests (i.e., conifers and aspens), mixed forests, grasses, and bare soil. Parameterization of these different land cover types is derived from the IGBP database (IGBP, 2018).

The subsurface of the study area is heterogeneous in both vertical and horizontal directions. The subsurface of the top 1 m corresponds to three soil layers as defined by the SSURGO database

and then corrected based on the land cover and geologic maps to include the outcropping of the bedrock. Two main types of soil are distinguished within the area: sandy loam and clay loam. The geology of the subsurface between 1 m and 8 m below the ground was defined with USGS maps, which were further improved by local knowledge by Pribulick et al., (2016). This subsurface region is highly heterogeneous with different formations such as crystalline, sedimentary rocks, unconsolidated rocks, alluvial deposits, and debris flow. The bottom layer of the domain (extending from 8 m below the ground surface to the bottom of the model) is assumed homogeneous and represents the fractured bedrock.

We simulated the water year (WY) 2015, a relatively average WY in the region based on average precipitation and temperature patterns. The meteorological forcing of the model has a resolution of an hour and is derived from two gridded datasets: PRISM and NLDAS. The PRISM dataset (Daly et al., 2008) is used for precipitation and temperature because of its accuracy and high spatial resolution (800m). However, the daily resolution of PRISM impedes its ability to be used to reproduce diurnal cycles, an important factor when studying land surface processes requiring hourly forcing. The phase 2 of the North America Land Data Assimilation System NLDAS-2 forcing (Cosgrove et al., 2003) on the contrary provides hourly changes in precipitation and temperature yet are only available at coarser, 1/8 degree, resolutions. As such, we employ a mass-conservative temporal interpolation, which disaggregates the total daily PRISM precipitation into an hourly time series based on the signal of the NLDAS-2 precipitation and temperature trends. For the other forcing variables (i.e., shortwave and longwave radiation, wind speed, atmospheric pressure, and specific humidity), we use NLDAS-2 forcing, (Cosgrove et al., 2003). Simulated river stages and SWE were compared to observations in previous studies (Maina et al., 2022; Foster and Maxwell, 2019). Groundwater measurements are scarce in the watershed and the

majority of the measurements are performed near a station measuring changes in river stages. Therefore, river stages and groundwater measurements at this point provide similar information.

2.2. Hillslopes delineation

As shown in Figure 1b, 127 hillslopes are delineated in the East River watershed based on the elevation following (Noël et al., 2014) and using Topotoolbox developed by (Schwanghart & Scherler, 2014). A threshold of flow accumulation was set to match the stream observations at major tributaries of the East River (Carroll et al., 2018). Because the hillslope delineation could be sensitive to the threshold of the drainage area, we tested different threshold values to find that the selected threshold value (810,000 m^2) represents the scale of hillslope at which the within-hillslope variability of key properties (such as elevation and aspect) is minimized and hillslope-averaged properties can account for the majority of watershed-scale variability (Wainwright et al., 2022).

2.3. Hillslopes clustering approaches

We use eight hillslope clustering approaches:

1. The ΔP_1 clustering, proposed in this study, identifies hillslopes with similar groundwater dynamics. Figure 2 shows the temporal variations of the simulated SWE and WTD at a selected hillslope (see its location in Figure 1). All hydrologic variables have been computed at a hillslope scale by computing the arithmetic average of all cells in each hillslope. In this mountainous watershed, where the largest changes in WTD are mostly a result of snowmelt, WTD decreases from the beginning of the WY (i.e., October) to the beginning of snowmelt (i.e., starting from April). As the snow starts to melt and precipitation starts to fall as rain instead of snow, WTD starts to rise. The shallowest WTD is June and July when the snow has completely melted and has had time to percolate

through the unsaturated zone into the groundwater. This period also corresponds to the period of high ET, because both the evaporative demand and the water availability are high. The dynamics show two periods characterize the dynamics of the hillslope: from the initial conditions to the baseflow conditions when the hillslope is losing water, then from baseflow conditions to the peak of WTD when the hillslope is gaining water. To characterize these groundwater dynamics, we define two variables:

- ΔP_1 represents the change in WTD between the beginning of the water year and the deepest WTD during the baseflow conditions. This variable quantifies the amount of water released by the hillslope during the dry period at the beginning of the water year. It thus contains information about the amount of water that the hillslope typically releases/loses, mainly by ET and discharge, given its physical characteristics and climate dynamics.
- ΔP_2 represents the changes in WTD between the peak flow (i.e., the period with the shallowest WTD) and the baseflow conditions. ΔP2 quantifies the amount of water gained in the hillslope by recharge, and thus contains information about the recharge ability of the hillslope given its physical characteristics and climate dynamics.

These two key variables allow us to quantify water release (ΔP_1) and recharge (ΔP_2) within a hillslope, two key dynamics of the watershed hydrologic function (Sivapalan, 2006; Wagener et al., 2007, Wainwright et al., 2022). We note that these dynamics are also illustrated by the changes in measured groundwater levels as depicted in Appendix A.

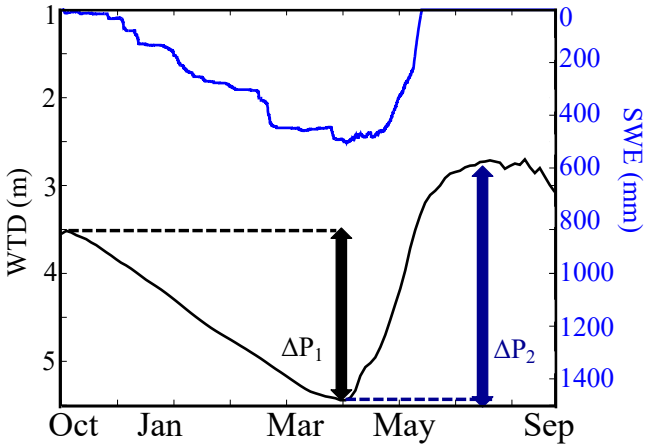

Figure 2: Temporal variations of water table depth (WTD) and SWE at an example hillslope. The location of the hillslope is shown in Figure 1.

2. Elevation: in mountainous watersheds, because the differences in hydroclimate are primarily driven by elevation, hillslopes with similar elevations could potentially have similar land surface processes signatures.
3. Land cover: hillslopes can also be clustered by their dominant land cover. Land cover shapes land surface processes, which in turn affect subsurface dynamics and the water balance at the hillslope scale.
4. TWI: The Topographic Wetness index commonly used to cluster hillslopes is given by: $ln\left(\frac{\alpha}{tan(\beta)}\right)$. Where α is the upslope draining area and β the local angle.
5. AI: the AI (ETP/Precipitation, where ETP is the potential evapotranspiration) represents the ratio of the average demand for moisture to the average supply of moisture. We derive the spatial distribution of the AI in the East River from the Global Aridity Index dataset (CGIAR-CSI, 2019).
6. Machine learning based clustering: we define the hillslope similarity using the clustering of ParFlow-CLM input and output data layers. Clustering was performed in three different

ways, using the following data: (1) model input (elevation, percentage of the main land cover type, TWI, and AI), referred to hereafter as the "clustering input" (C.I.) method, (2) model output (ET, SWE, WTD, and ΔP_1), referred to hereafter as the "clustering output" (C.O.) method, and (3) both model input and output data layers, referred to hereafter as the "clustering input-output" (C.I.O.) method. We use hierarchical clustering, which is a decision-tree-based method that divides data points based on a series of binary splits (Devadoss et al., 2020; Kassambara, 2017; Wainwright et al., 2022). We define the linkage (or the distance) between any two clusters based on the Euclidian distance and the Ward method that computes the variance within each cluster, measuring the distance between each observation and the cluster's mean, and then taking the sum of the distances' squares.

2.4. Hillslope clustering comparisons

To test the ability of the eight selected clustering approaches to identify and categorize hillslopes with similar static characteristics and dynamics, we assess each clustering's ability to describe several characteristics of the hillslope: elevation, land cover, hydroclimate (i.e., precipitation), land surface processes (SWE and ET), and subsurface dynamics (WTD values and variations). For each clustering, we define three zones. For each variable, zone, and clustering, we compute the mean (μ) of the hillslope values and the corresponding coefficient of variation (CV). We also calculate the mean of the CV of the different zones for each variable and clustering.

3. Results

3.1.Hillslope characteristics

Figure 3 shows the spatial distribution of hillslope temperature, precipitation, SWE, ET, WTD, and ΔP_1.

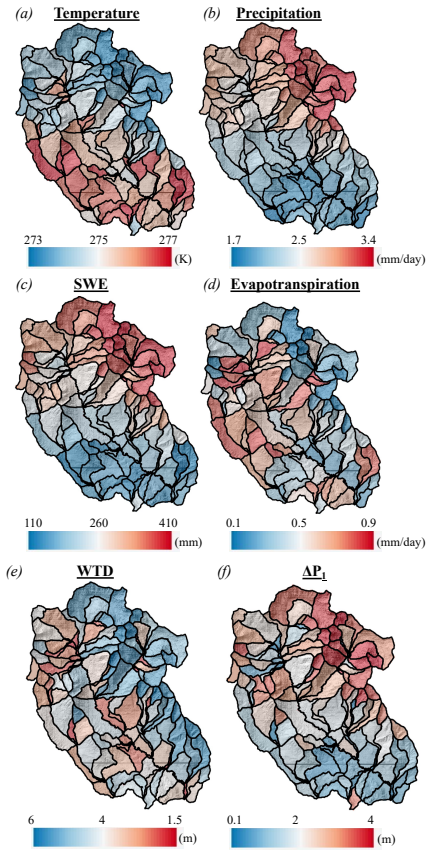

312

313 Figure 3: Spatial distributions of hillslope annual average values of (a) temperature, (b)
314 precipitation, (c) snow water equivalent (SWE), (d) evapotranspiration, (e) water table depth
315 (WTD) and (e) ΔP_1

316 As expected, the hillslopes characterized by high SWE have high precipitation and low
317 temperatures in contrast to the hillslopes with low SWE. However, ET shows a different pattern,
318 because it depends on both water availability and ET demands, which depends on the type of land
319 cover. The mid-elevation zone (i.e., zone 2) with a high coverage of forests has high ET. Hillslope
320 with high ΔP_1 have a deep WTD on average, this is because the WTD increases significantly during
321 baseflow conditions and reaches very large values as quantified by ΔP_1. Hillslopes with high ΔP_1
322 values generally correspond to hillslopes with high precipitation and low temperature and therefore
323 high SWE values.

To better understand the relationship between ΔP_1 and the hillslope physical characteristics and hydrologic processes, we study the Pearson correlation coefficient between ΔP_1 and the elevation, the percent of the dominant land cover, TWI, AI, ET, SWE, and WTD (Figure 4).

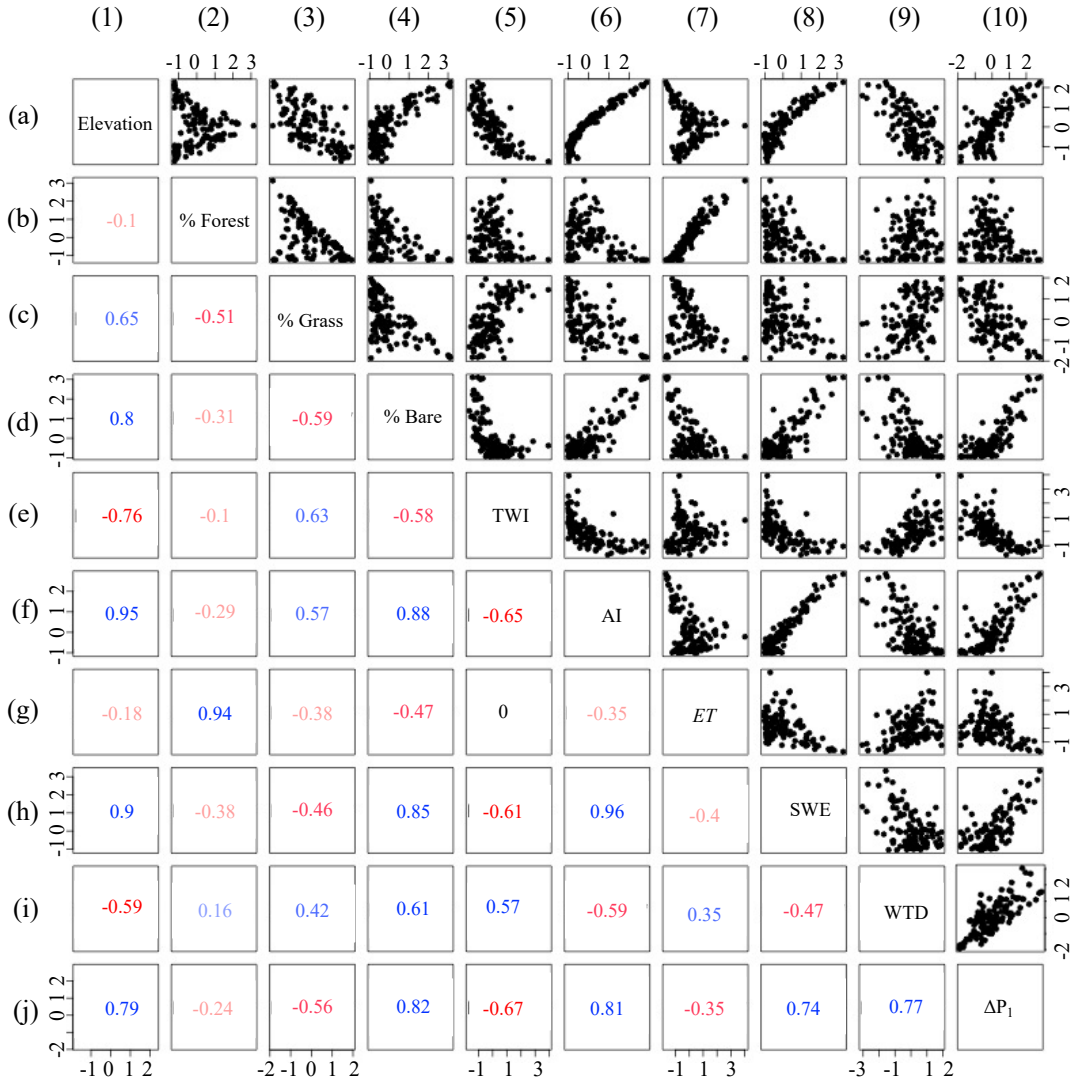

Figure 4: Pearson's correlations between the selected variables for hillslope clustering approaches: elevation, percent of the main land cover type (forest, grassland, and bare soil), topographic wetness index (TWI), aridity index (AI), evapotranspiration (ET), snow water equivalent (SWE), water table depth (WTD), and seasonal changes in groundwater ΔP_1. Note that correlation coefficients are colored coded based on their values.

Results for ΔP_2 are not shown because ΔP_2 is strongly correlated to ΔP_1. Bare soil, TWI, AI, SWE, and ΔP_1 are strongly correlated (we define this as Pearson's correlation coefficient higher than 0.7) with elevation (Figure 4, column 1, lines d, e, f, h, and j). In particular, elevation has a dominant control on AI and SWE with a Pearson's correlation coefficient higher than 0.9. We observe nonlinearity such that TWI increases in the lower elevation and that AI becomes constant at the lower elevation. High percentage of forests is only found in mid-elevation (Figure 4, 2a) whereas high percentage of grassland is well correlated to low elevations (Figure 4, 3a). ET is positively correlated to the percent of forests (Pearson's correlation coefficient is higher than 0.9, Figure 4 2g). ΔP_1 has a Pearson's correlation coefficient higher than 0.7 for 6 out of 9 studied variables (elevation, percent of bare soil, TWI (correlation coefficient equal to 0.67), AI, SWE, and WTD, Figure 4, line j, columns 1, 4, 5, 6, 8 and 9); it, therefore, indicates that changes ΔP_1 can reflect the changes of these variables. The two variables with low correlations with ΔP_1 are ET and the percent of forests (Figure 4, line j, column 2 and 7). ET is related to groundwater dynamics in a nonlinear way (Condon et al., 2013; Ferguson & Maxwell, 2010; Rahman et al., 2016). As shown in these studies, regions with shallow WTDs have the highest ET fluxes and this flux typically decreases significantly with WTD. When WTD reaches a critical depth, the groundwater and the atmosphere disconnect and changes in WTD do not impact ET.

3.2.Hillslopes clustering

For each clustering, we identify three zones (Figure 5). For the ΔP_1, elevation, TWI, and AI clustering approaches, we define the thresholds of each zone by analyzing the distributions of the hillslope values of these indices.

1. ΔP_1: Zone 1 comprises hillslopes whose ΔP_1 are less than 1.5 m, ΔP_1 of hillslopes of zone 2 are comprised between 1.5 m and 2.5 m, and Zone 3 group all hillslopes with ΔP_1 greater than 2.5 m.

1. Elevation: Zone 1 characterizes low elevation areas (average hillslope elevation less than 3000 m), Zone 2 mid (average hillslope elevation comprises between 3000 m and 3500 m), and Zone 3 high elevation (hillslope with an average elevation greater than 3500 m).

3. Land Cover: Zone 1 describes hillslopes that have predominantly grasses as land cover, Zone 2 for hillslopes with more than 50% of forest, and Zone 3 for hillslopes where bare soil is the dominant land cover.

4. TWI: We define 3 zones with high (TWI>1, Zone 1), mid (TWI comprises between 1 and 0.2 Zone 2), and low (TWI<0.2, Zone 3) TWI.

5. AI: Zone 1 comprises hillslopes with AI less than 0.45, Zone 2 describes hillslopes with AI between 0.45 and 0.55, and hillslopes of Zone 3 have an AI greater than 0.55.

6. Machine learning based clustering: the approaches automatically regroup the similar hillslopes into three zones.

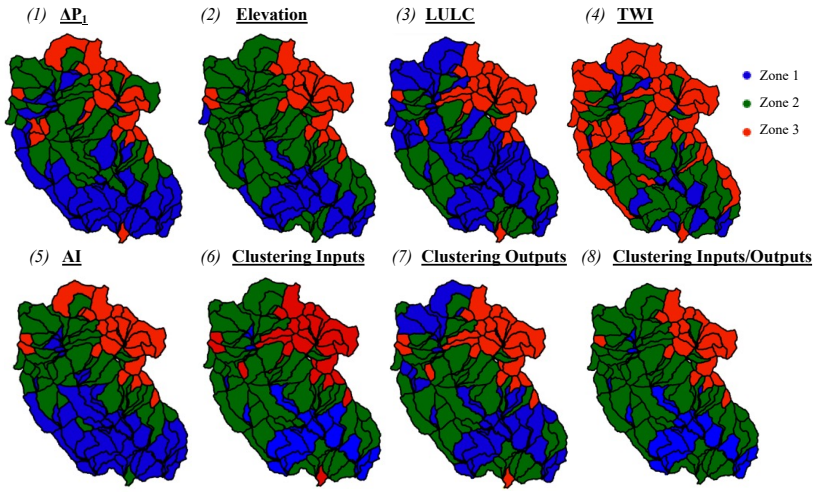

Figure 5: Spatial distribution of hillslope zones derived from the eight selected clustering approaches (1) ΔP_1, (2) elevation, (3) land cover (LULC), (4) topographic wetness index (TWI),

373 (5) aridity index (AI), and clustering with (6) inputs, (7) outputs, and (8) inputs and outputs
374 variables.

375 **3.3.Comparisons of the eight selected hillslope clustering approaches**
376 Table 1 depicts the mean (μ) and the corresponding coefficient of variation (CV) of
377 hillslope values for each variable, zone, and clustering.

378

Variable: Elevation			
ΔP_1	**Elevation**	**LULC**	**TWI**
Zone 1: μ=3027 ; CV=0.25 Zone 2: μ=3226 ; CV=0.06 Zone 3: μ=3593 ; CV=0.04	Zone 1: μ=2884 ; CV=0.02 Zone 2: μ=3233 ; CV=0.06 Zone 3: μ=3641 ; CV=0.04	Zone 1: μ=3099 ; CV=0.06 Zone 2: μ=3065 ; CV=0.16 Zone 3: μ=3595 ; CV=0.04	Zone 1: μ=2853 ; CV=0.25 Zone 2: μ=2637 ; CV=0.41 Zone 3: μ=1999 ; CV=0.84
AI	**Clustering Input**	**Clustering Output**	**Clustering I. O.**
Zone 1: μ=2947 ; CV=0.03 Zone 2: μ=3285 ; CV=0.03 Zone 3: μ=3625 ; CV=0.03	Zone 1: μ=3202 ; CV=0.04 Zone 2: μ=2903 ; CV=0.03 Zone 3: μ=3592 ; CV=0.03	Zone 1: μ=3029 ; CV=0.07 Zone 2: μ=3175 ; CV=0.04 Zone 3: μ=3605 ; CV=0.03	Zone 1: μ=3232 ; CV=0.049 Zone 2: μ=2904 ; CV=0.034 Zone 3: μ=3658 ; CV=0.025
Variable: Precipitation			
ΔP_1	**Elevation**	**LULC**	**TWI**
Zone 1: μ=2.24 ; CV=0.21 Zone 2: μ=2.68 ; CV=0.18 Zone 3: μ=3.26 ; CV=0.15	Zone 1: μ=2.11 ; CV=0.22 Zone 2: μ=2.77 ; CV=0.22 Zone 3: μ=3.55 ; CV=0.09	Zone 1: μ=2.42 ; CV=0.22 Zone 2: μ=2.39 ; CV=0.20 Zone 3: μ=3.26 ; CV=0.16	Zone 1: μ=2.38 ; CV=0.23 Zone 2: μ=2.37 ; CV=0.22 Zone 3: μ=2.74 ; CV=0.23
AI	**Clustering Input**	**Clustering Output**	**Clustering I. O.**
Zone 1: μ=2.10 ; CV=0.15 Zone 2: μ=2.74 ; CV=0.17 Zone 3: μ=3.39 ; CV=0.12	Zone 1: μ=2.68 ; CV=0.18 Zone 2: μ=2.06 ; CV=0.16 Zone 3: μ=3.41 ; CV=0.11	Zone 1: μ=2.33 ; CV=0.22 Zone 2: μ=2.63 ; CV=0.18 Zone 3: μ=3.43 ; CV=0.11	Zone 1: μ=2.73 ; CV=0.18 Zone 2: μ=2.07 ; CV=0.17 Zone 3: μ=3.56 ; CV=0.06
Variable: Temperature			
ΔP_1	**Elevation**	**LULC**	**TWI**
Zone 1: μ=276.5 ; CV=0.001 Zone 2: μ=275.9 ; CV=0.002 Zone 3: μ=274.5 ; CV=0.002	Zone 1: μ=276.2 ; CV=0.003 Zone 2: μ=276.0 ; CV=0.003 Zone 3: μ=274.1 ; CV=0.002	Zone 1: μ=276.1 ; CV=0.002 Zone 2: μ=276.4 ; CV=0.001 Zone 3: μ=274.4 ; CV=0.002	Zone 1: μ=276.3 ; CV=0.001 Zone 2: μ=276.2 ; CV=0.002 Zone 3: μ=275.6 ; CV=0.003
AI	**Clustering Input**	**Clustering Output**	**Clustering I. O.**
Zone 1: μ=276.6 ; CV=0.001 Zone 2: μ=275.8 ; CV=0.002 Zone 3: μ=274.3 ; CV=0.002	Zone 1: μ=276.2 ; CV=0.002 Zone 2: μ=276.5 ; CV=0.001 Zone 3: μ=274.4 ; CV=0.003	Zone 1: μ=276.2 ; CV=0.002 Zone 2: μ=276.3 ; CV=0.002 Zone 3: μ=274.3 ; CV=0.002	Zone 1: μ=276.1 ; CV=0.002 Zone 2: μ=276.5 ; CV=0.001 Zone 3: μ=274.1 ; CV=0.002
Variable: SWE			

ΔP_1	Elevation	LULC	TWI
Zone 1: μ=152 ; CV=0.30 Zone 2: μ=204 ; CV=0.34 Zone 3: μ=335 ; CV=0.31	Zone 1: μ=149 ; CV=0.38 Zone 2: μ=201 ; CV=0.43 Zone 3: μ=389 ; CV=0.26	Zone 1: μ=181 ; CV=0.34 Zone 2: μ=151 ; CV=0.29 Zone 3: μ=339 ; CV=0.29	Zone 1: μ=169 ; CV=0.50 Zone 2: μ=165 ; CV=0.39 Zone 3: μ=234 ; CV=0.46
AI	**Clustering Input**	**Clustering Output**	**Clustering I. O.**
Zone 1: μ=137 ; CV=0.18 Zone 2: μ=206 ; CV=0.25 Zone 3: μ=360 ; CV=0.24	Zone 1: μ=191 ; CV=0.32 Zone 2: μ=145 ; CV=0.17 Zone 3: μ=359 ; CV=0.25	Zone 1: μ=173 ; CV=0.34 Zone 2: μ=179 ; CV=0.30 Zone 3: μ=365 ; CV=0.23	Zone 1: μ=200 ; CV=0.33 Zone 2: μ=146 ; CV=0.20 Zone 3: μ=396 ; CV=0.18

Variable: ET

ΔP_1	Elevation	LULC	TWI
Zone 1: μ=0.42 ; CV=0.47 Zone 2: μ=0.41 ; CV=0.47 Zone 3: μ=0.17 ; CV=0.74	Zone 1: μ=0.35 ; CV=0.75 Zone 2: μ=0.48 ; CV=0.54 Zone 3: μ=0.15 ; CV=0.90	Zone 1: μ=0.31 ; CV=0.36 Zone 2: μ=0.61 ; CV=0.27 Zone 3: μ=0.19 ; CV=0.69	Zone 1: μ=0.37 ; CV=0.58 Zone 2: μ=0.41 ; CV=0.49 Zone 3: μ=0.35 ; CV=0.56
AI	**Clustering Input**	**Clustering Output**	**Clustering I. O.**
Zone 1: μ=0.40 ; CV=0.46 Zone 2: μ=0.45 ; CV=0.45 Zone 3: μ=0.14 ; CV=0.58	Zone 1: μ=0.49 ; CV=0.37 Zone 2: μ=0.25 ; CV=0.32 Zone 3: μ=0.19 ; CV=0.68	Zone 1: μ=0.27 ; CV=0.29 Zone 2: μ=0.55 ; CV=0.29 Zone 3: μ=0.18 ; CV=0.65	Zone 1: μ=0.48 ; CV=0.38 Zone 2: μ=0.25 ; CV=0.31 Zone 3: μ=0.12 ; CV=0.57

Variable: Saturation

ΔP_1	Elevation	LULC	TWI
Zone 1: μ=0.77 ; CV=0.14 Zone 2: μ=0.69 ; CV=0.10 Zone 3: μ=0.66 ; CV=0.11	Zone 1: μ=0.75 ; CV=0.23 Zone 2: μ=0.73 ; CV=0.16 Zone 3: μ=0.67 ; CV=0.13	Zone 1: μ=0.75 ; CV=0.14 Zone 2: μ=0.71 ; CV=0.15 Zone 3: μ=0.68 ; CV=0.09	Zone 1: μ=0.81 ; CV=0.14 Zone 2: μ=0.72 ; CV=0.12 Zone 3: μ=0.70 ; CV=0.13
AI	**Clustering Input**	**Clustering Output**	**Clustering I. O.**
Zone 1: μ=0.75 ; CV=0.15 Zone 2: μ=0.73 ; CV=0.13 Zone 3: μ=0.68 ; CV=0.11	Zone 1: μ=0.72 ; CV=0.11 Zone 2: μ=0.77 ; CV=0.16 Zone 3: μ=0.69 ; CV=0.09	Zone 1: μ=0.76 ; CV=0.15 Zone 2: μ=0.72 ; CV=0.10 Zone 3: μ=0.68 ; CV=0.09	Zone 1: μ=0.72 ; CV=0.10 Zone 2: μ=0.78 ; CV=0.15 Zone 3: μ=0.66 ; CV=0.08

Variable: WTD

ΔP_1	Elevation	LULC	TWI
Zone 1: μ=2.9 ; CV=0.06 Zone 2: μ=3.7 ; CV=0.05 Zone 3: μ=4.8 ; CV=0.07	Zone 1: μ=3.4 ; CV=0.1 Zone 2: μ=3.2 ; CV=0.07 Zone 3: μ=4.6 ; CV=0.08	Zone 1: μ=3.0 ; CV=0.06 Zone 2: μ=3.5 ; CV=0.07 Zone 3: μ=4.7 ; CV=0.07	Zone 1: μ=2.4 ; CV=0.04 Zone 2: μ=3.3 ; CV=0.04 Zone 3: μ=4.0 ; CV=0.1
AI	**Clustering Input**	**Clustering Output**	**Clustering I. O.**
Zone 1: μ=3.1 ; CV=0.06 Zone 2: μ=3.5 ; CV=0.07 Zone 3: μ=4.7 ; CV=0.08	Zone 1: μ=3.2 ; CV=0.04 Zone 2: μ=2.6 ; CV=0.04 Zone 3: μ=4.4 ; CV=0.06	Zone 1: μ=2.8 ; CV=0.05 Zone 2: μ=3.2 ; CV=0.04 Zone 3: μ=4.5 ; CV=0.05	Zone 1: μ=3.3 ; CV=0.04 Zone 2: μ=2.5 ; CV=0.04 Zone 3: μ=4.8 ; CV=0.05

Variable: ΔP_2

ΔP_1	Elevation	LULC	TWI
Zone 1: μ=2.9 ; CV=0.06	Zone 1: μ=3.4 ; CV=0.1	Zone 1: μ=3.0 ; CV=0.06	Zone 1: μ=2.4 ; CV=0.04
Zone 2: μ=3.7 ; CV=0.05	Zone 2: μ=3.2 ; CV=0.07	Zone 2: μ=3.5 ; CV=0.07	Zone 2: μ=3.3 ; CV=0.04
Zone 3: μ=4.8 ; CV=0.07	Zone 3: μ=4.6 ; CV=0.08	Zone 3: μ=4.7 ; CV=0.07	Zone 3: μ=4.0 ; CV=0.1
AI	**Clustering Input**	**Clustering Output**	**Clustering I. O.**
Zone 1: μ=3.1 ; CV=0.06	Zone 1: μ=3.2 ; CV=0.04	Zone 1: μ=2.8 ; CV=0.05	Zone 1: μ=3.3 ; CV=0.04
Zone 2: μ=3.5 ; CV=0.07	Zone 2: μ=2.6 ; CV=0.04	Zone 2: μ=3.2 ; CV=0.04	Zone 2: μ=2.5 ; CV=0.04
Zone 3: μ=4.7 ; CV=0.08	Zone 3: μ=4.4 ; CV=0.06	Zone 3: μ=4.5 ; CV=0.05	Zone 3: μ=4.8 ; CV=0.05

Table 1: Mean μ and coefficient of variation CV of each variable and hillslope zone derived from the 8 clustering approaches.

3.1.1. Similarities in hillslope structure

Elevation plays an important role in the hydroclimate of a region especially in mountainous watersheds where it controls snow accumulation and controls the downstream hydrology. Figure 6 shows the elevation frequency distributions associated with the 3 zones derived from the 8 clustering approaches.

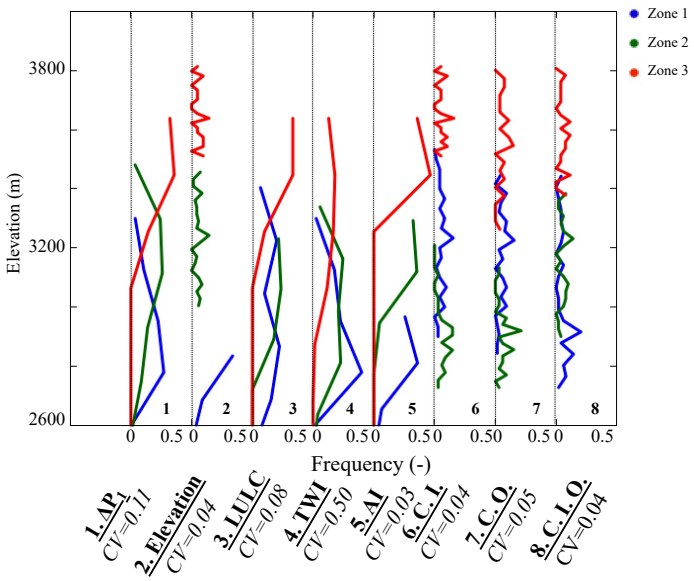

Figure 6: Frequency distributions of hillslope elevation. Clustering approaches are based on ΔP_1, elevation, land cover (LULC), topographic wetness index (TWI), aridity index (AI), and

390 machine-learning approaches (with inputs C.I., outputs C.O., and inputs and outputs C.I.O).
391 Hillslope clustering approaches are located across the x-axis. Note that we plotted the distributions
392 of the 8 clustering approaches on the same graph, between each dotted line (frequency from 0 to
393 0.5) are plotted the frequency distributions of the three zones derived from the clustering.
394
395 By classifying the hillslopes using their similarity in ΔP_1, we observe that hillslopes with
396 low ΔP have the lowest elevation while the hillslopes of zone 3 (high ΔP_1) have the highest
397 elevation. Unsurprisingly, the second clustering (i.e. elevation) clearly identifies the hillslopes with
398 similar elevation. The AI clustering also identifies hillslopes with similar elevation as shown in
399 Figures 4 and 6. The TWI clustering performs moderately, where zones 1 and 2 are characterized
400 by similar elevation distributions. Hillslopes with lower TWI are mostly located in high elevation
401 areas on the contrary to the low elevation hillslopes. In the land cover clustering, most of the
402 grassed hillslopes (zone 1) are in low elevation, forests (zone 2) in mid-elevation, and hillslopes
403 whose landscape is mainly bare soil (zone 3) are in high elevation areas above the tree line. The
404 three clustering approaches using machine learning allow identifying hillslopes with similar
405 elevation, their coefficients of variation are of the same order as the elevation clustering.
406 Table 2 describes the average hillslope ratio of land cover type (forests, grassland, and bare
407 soil) for each zone and type of clustering. The land cover clustering indicates that grassland is the
408 dominant land cover of zone 1, forests Zone 2, and bare soil zone 3. Only the machine learning
409 clustering approaches using outputs lead to a similar conclusion whereas while the other clustering
410 approaches capture the characteristics of zone 1 and 3, they do not identify a distinct forested zone
411 2. For the ΔP_1 clustering this could be attributed to the disconnection between groundwater
412 dynamics and land surface processes that takes place in certain forested zones. Since clustering

based on landscape characteristics and ΔP_1 do not identify such a distinct zone, it suggests that this zone may not be indicative of distinct hydrologic behavior.

ΔP_1	Forest	Grassland	Bare Soil
Zone 1	0.35	0.55	0.10
Zone 2	0.35	0.43	0.22
Zone 3	0.11	0.27	0.62
CV	0.97	0.56	0.69
Elevation	**Forest**	**Grassland**	**Bare Soil**
Zone 1	0.28	0.56	0.15
Zone 2	0.41	0.42	0.17
Zone 3	0.07	0.26	0.68
CV	1.33	0.76	1.07
Land Cover	**Forest**	**Grassland**	**Bare Soil**
Zone 1	0.23	0.67	0.14
Zone 2	0.72	0.26	0.12
Zone 3	0.12	0.22	0.66
CV	0.67	0.45	0.64
Topographic Wetness Index (TWI)	**Forest**	**Grasslands**	**Bare Soil**
Zone 1	0.24	0.66	0.10
Zone 2	0.35	0.51	0.14
Zone 3	0.32	0.35	0.33
CV	1.47	0.49	0.95
Aridity Index	**Forest**	**Grassland**	**Bare Soil**
Zone 1	0.34	0.57	0.09
Zone 2	0.37	0.41	0.22
Zone 3	0.07	0.32	0.61
CV	0.91	0.56	0.69
Clustering with input layers	**Forest**	**Grassland**	**Bare Soil**
Zone 1	0.44	0.42	0.14
Zone 2	0.11	0.83	0.06
Zone 3	0.12	0.25	0.63
CV	0.83	0.38	0.62

Clustering with output layers	**Forest**	**Grasslands**	**Bare Soil**
Zone 1	0.14	0.77	0.09
Zone 2	0.52	0.34	0.15
Zone 3	0.11	0.25	0.64
CV	0.77	0.38	0.61
Clustering with inputs and outputs	**Forest**	**Grassland**	**Bare Soil**
Zone 1	0.42	0.40	0.18
Zone 2	0.12	0.82	0.06
Zone 3	0.05	0.24	0.70
CV	0.87	0.41	0.65

Table 2: Average values of hillslope ratio of forests, grasslands, and bare soils for each zone and clustering.

3.1.2. Similarities in hydroclimate

Figures 7a and b depict the distributions of precipitation and temperature obtained with the eight selected clustering approaches. The AI clustering allows identifying hillslope with similar hydroclimate because it has low values of coefficients of variation. Zone 1 located in low elevation has low precipitation and high temperatures, contrary to zone 3. Zone 2 is characterized by a hydroclimate that is in between those of Zone 1 and 3. Our ΔP_1 clustering leads to conclusions similar to the machine learning based clustering and AI. These three clustering approaches have the same average CV and are the only methods that allow identifying hillslopes with similar hydroclimate. Although, we note that in the three machine learning based clustering as well as in the ΔP clustering, Zones 1 and 2 have similar hydroclimate, which is not the case in the AI clustering. While the land cover clustering approaches clearly identifies the typical hydroclimate of the hillslopes of zone 3, the two remaining zones have the same hydroclimate. The TWI clustering does not identify hillslopes with similar hydroclimates because it relies on the hydrologic processes driven by the topography. TWI shows that clustering that includes only

hydroclimate would miss important information on distinct hillslope hydrologic processes that strongly affect the response of the hillslope to meteorological forcing.

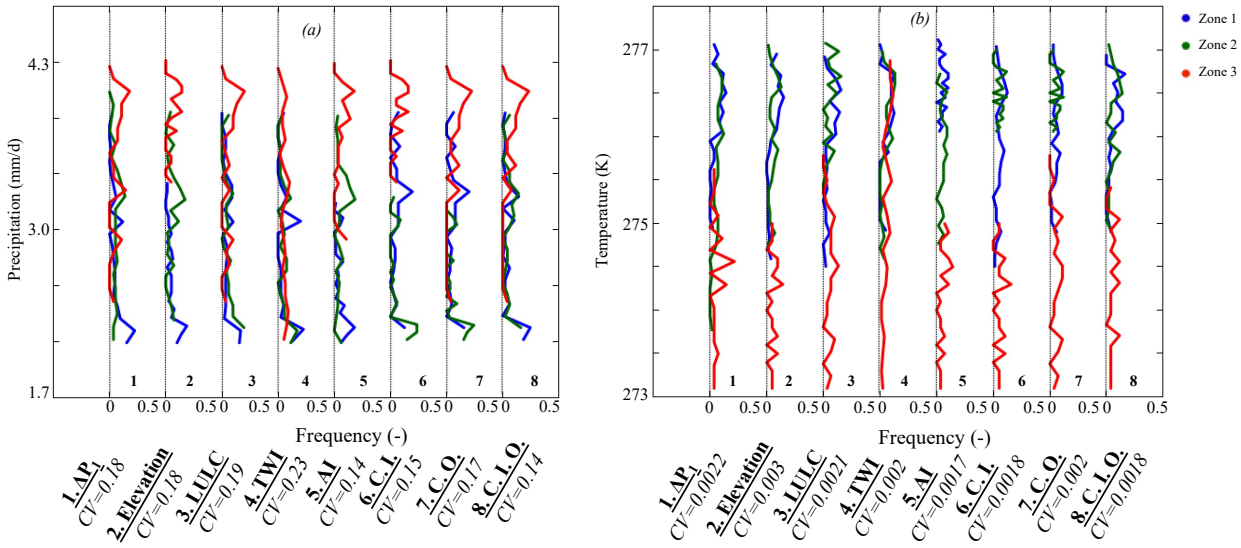

Figure 7: Frequency distributions of hillslope (a) annual average daily rates of precipitation and (b) annual average temperature. Clustering approaches are based on ΔP_1, elevation, land cover (LULC), topographic wetness index (TWI), aridity index (AI), and machine-learning approaches (with inputs C.I., outputs C.O., and inputs and outputs C.I.O). Hillslope clustering approaches are located across the x-axis. Note that we plotted the distributions of the 8 clustering approaches on the same graph, between each dotted line (frequency from 0 to 0.5) are plotted the frequency distributions of the three zones derived from the clustering.

3.1.3. Similarities in hydrologic processes

In this section, we study the ability the selected clustering approaches to identify hillslopes with similar hydrologic processes: snow dynamics, evapotranspiration, and WTD values and variations.

3.1.3.1. Land surface processes

A robust clustering in mountainous watersheds should identify hillslopes with similar snow dynamics. Figure 8a illustrates the SWE frequency distribution associated with each zone and clustering. Because SWE dynamics are primarily driven by elevation and the precipitation, the AI and machine learning based clustering have the lowest average of the CV followed by the land cover and the ΔP_1 clustering. The land cover spatial distribution contains information about elevation especially in high elevation areas where some hillslopes are located above the tree line. The ΔP_1 clustering accounts for SWE dynamics because ΔP_1 is highly correlated to SWE as discussed in section 3.1.

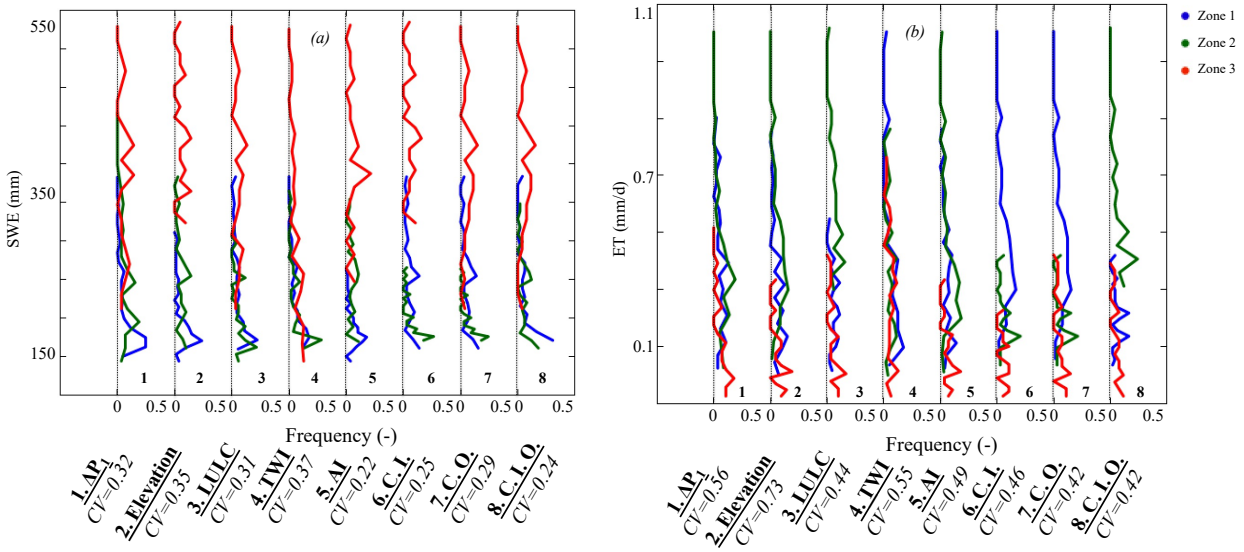

Figure 8: Frequency distributions of hillslope land surface variables (a) annual average SWE and (b) annual average daily rates of ET. Clustering approaches are based on ΔP_1, elevation, land cover (LULC), topographic wetness index (TWI), aridity index (AI), and machine-learning approaches (with inputs C.I., outputs C.O., and inputs and outputs C.I.O). Hillslope clustering approaches are located across the x-axis. Note that we plotted the distributions of the 8 clustering approaches on the same graph, between each dotted line (frequency from 0 to 0.5) are plotted the frequency distributions of the three zones derived from the clustering.

The spatial distribution of ET is controlled by many factors, including soil moisture, land cover, and subsurface flow. The land cover clustering performs well at identifying hillslopes with similar ET because the latter strongly depends on the land cover (Figure 8b). Consistent with the aforementioned results, the other clustering approaches performing well are the machine learning based clustering and the AI. The TWI and elevation clustering approaches do not separate hillslopes by their ET values because they do not account for varying land cover and soil properties that influence ET. The average CV of the ΔP_1 clustering is close to those of the land cover and AI clustering. As stated in many studies (Ferguson & Maxwell, 2010; Maina & Siirila-Woodburn, 2020, Maina et al., 2022), subsurface flow affects ET, as such information about subsurface flow contains valuable information about the ET even if the correlation between ΔP_1 and ET is nonlinear.

3.1.3.2.Similarities in subsurface hydrodynamics

We investigate the ability of the eight selected clustering approaches to identify hillslopes with similar subsurface hydrodynamics. We study the average saturation of the first 10 cm of the soil throughout the WY, the yearly average of WTD and ΔP_2. Soil saturation is a key feature in both subsurface and atmospheric dynamics; it controls ET and groundwater recharge. The averages CV of the ΔP_1, TWI, AI, land cover, and clustering approaches are very similar (Figure 9a). As the land cover clustering adequately regroup hillslopes with similar ET, it also allows regrouping hillslopes with similar soil saturation. Because the TWI describes the characteristics that drive flow, it serves as a good indicator of soil saturation like the AI. Similar to the results above, the machine learning based clustering perform well. The ΔP_1 clustering has a low average CV due to the strong connection between the changes in WTD and soil saturation. It is only the elevation

clustering that fails to identify hillslope with similar soil saturation, where the distributions of the three defined zones show overlap.

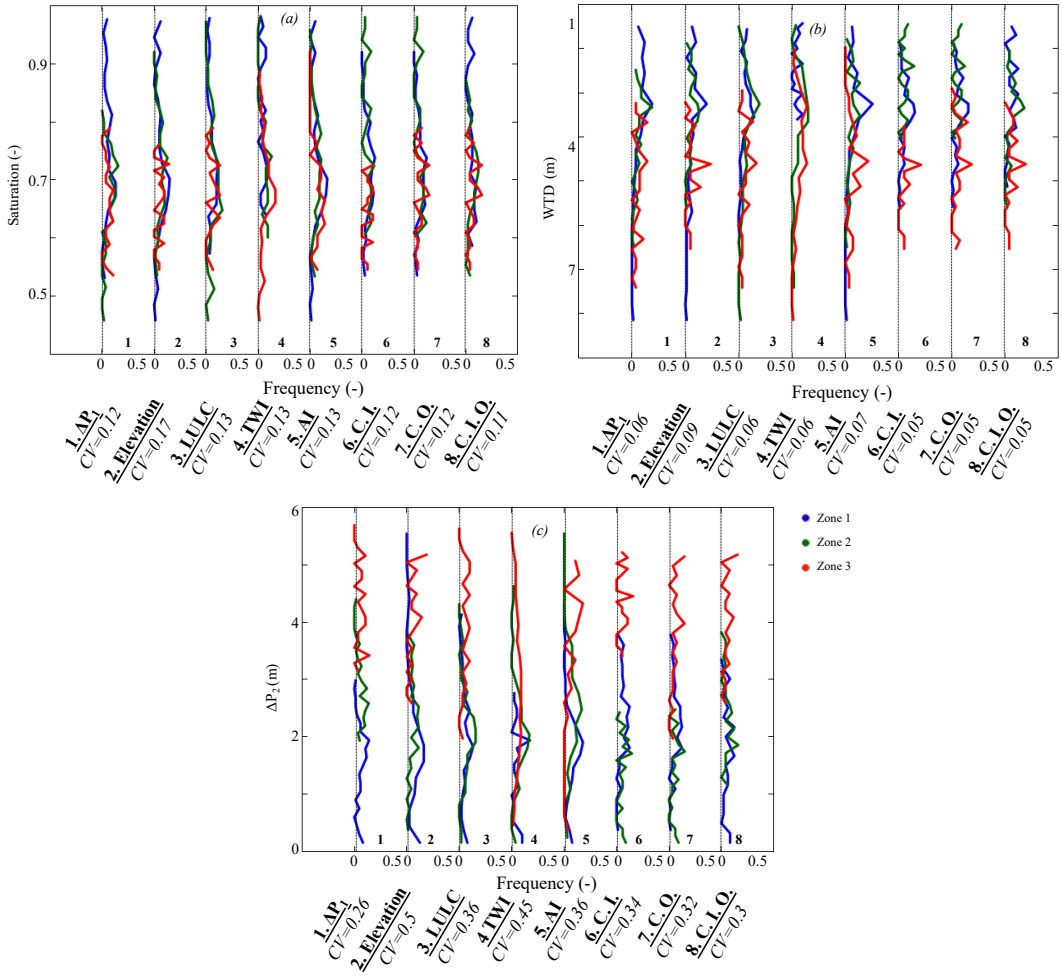

Figure 9: Frequency distributions of hillslope (a) saturation, (b) WTD, and (c) ΔP_2. Clustering approaches are based on ΔP_1, elevation, land cover (LULC), topographic wetness index (TWI), aridity index (AI), and machine-learning approaches (with inputs C.I., outputs C.O., and inputs and outputs C.I.O). Hillslope clustering approaches are located across the x-axis. Note that we plotted the distributions of the 8 clustering approaches on the same graph, between each dotted line (frequency from 0 to 0.5) are plotted the frequency distributions of the three zones derived from the clustering.

WTD is an important variable for determining groundwater storage. Here, we rely on the average WTD throughout the year. As expected, the ΔP_1 clustering identifies hillslopes with similar WTD (Figure 9b). Zone 1 located in low elevation has the shallowest WTD and the lowest ΔP_1, contrary to zone 3. Zone 2 exhibits a behavior that is in between those of Zone 1 and 3. The TWI and land cover clustering approaches also are good for identifying hillslope with similar WTD. Hillslopes with low TWI (Zone 3) have the deepest WTD, contrary to the hillslopes of Zone 1. The TWI identifies hillslopes with similar WTD because of the high relief of the watershed that drive its hydrology (Fan et al., 2019). The land cover clustering indicates that most of the forest (Zone 2) and bare soil (Zone 3) hillslopes have deep WTD whereas grasses (Zone 1) hillslopes have the shallowest WTD. The elevation clustering doesn't accurately identify hillslopes with similar WTD, and its average CV remains higher than the 4 other clustering approaches. The AI, like the elevation, isn't a good variable for identifying hillslopes with similar WTD. All their three zones overlap in terms of WTD. Results from the machine learning based clustering are similar to the ΔP_1 clustering with a CV of the same order, yet there isn't a clear distinction between Zone 1 and 2 in these machine learning based clustering approaches.

Figure 9c illustrates the distributions of the ΔP_2 for each clustering approach and zone. ΔP_1 clusters hillslopes with similar ΔP_2 as expected. Another suitable clustering approach for hillslopes with similar ΔP_2 is the land cover. Zone 3 characterizing bare soil hillslopes has the highest ΔP_2, unlike zones 1 and 2. The AI clustering shows that the majority of zone 3 hillslopes have high ΔP_2 whereas zone 2 hillslopes have low ΔP_2, followed by zone 1 hillslopes. In terms of ΔP_2 similarity, the elevation clustering outperforms the TWI. The machine learning based clustering approaches are good for identifying hillslopes with similar ΔP_2 especially the clustering using inputs variables

(CI). The two other machine learning based clustering approaches (outputs and inputs and outputs) do not distinguish zone 1 from zone 2.

4. Discussions

In this section, we discuss the advantages of the proposed ΔP clustering compared to the other clustering approaches and its ability to capture dry and wet hydrologic conditions.

4.1. Advantages of the ΔP clustering

Depending on the purpose of the identification of similar hillslopes, the appropriate clustering may change. Nonetheless, it is important for any clustering approach to identify hillslopes with similar hydrologic processes. As demonstrated here, the advantage of using ΔP_1 to identify similar hillslopes is that many hydrologic processes are embedded in ΔP_1. Our comparisons have shown that by using a ΔP_1 clustering, one is able to identify hillslopes with not only similar subsurface hydrodynamics but also similar land surface processes. Because these processes are intimately linked to the physical characteristics of the hillslope, its hydroclimate, and its land cover, the ΔP_1 clustering also allows for the identification of hillslopes with the aforementioned characteristics similar.

We, however, highlight that other clustering approaches may outperform the ΔP_1 when looking at a single characteristic. For instance, our results show that the elevation and AI (or other clustering approaches based on the hydroclimate e.g., Carrillo et al., 2011) clustering approaches may be excellent at identifying hillslopes with similar hydroclimates and snow dynamics. The land cover clustering allows for better identification of hillslopes with similar land surface processes such as ET and soil saturation. Lastly, the TWI clustering (e.g., Beven & Kirby, 1979; Grabs et al., 2009; Hjerdt et al., 2004; Loritz et al., 2019) allows the identification of hillslopes with similar groundwater dynamics and soil saturation values as it describes the topographic flow. In terms of

overall performance, our results show that for the study site considered here, the machine learning based clustering approaches are also a very good at identifying similar hillslopes.

Wainwright et al., (2022) use an unsupervised clustering method and remote sensing data layers which include elevation, SWE, radiation, resistivity, and Normalized Difference Vegetation Index NDVI to define 7 clusters in the East River watershed. While their clustering method has more zones (7) than ours (3), it leads to similar conclusions as our study where zones 1 and 2 are characterized by low elevation, high TWI, and low SWE values contrary to zones 5 and 6.

Other hillslope clustering approaches based on hydrologic processes relied on the Peclet number (Berne et al., 2005; S. W. Lyon & Troch, 2007; Steve W. Lyon & Troch, 2010) which describes the subsurface hydrological response and is derived from an analytical solution of the subsurface flow (e.g. the Boussinesq storage equation (Steve W. Lyon & Troch, 2010)). However, while the three-dimensional Richards equation has the advantage of better representing the subsurface flow it cannot be solved analytically, hence these indices cannot be applied to integrated hydrologic models. Our approach has demonstrated that the ΔP helps quantify the subsurface hydrologic responses without using these indices and therefore overcomes the limitation of the use of attributes such as the Peclet number on integrated hydrologic models to categorize hillslopes.

4.2.Similarities in hydrologic responses to wet and dry conditions

According to McDonnell & Woods, (2004) and Wagener et al., (2007), any classification should be able to predict the dynamics of the hillslopes. We test the ability of the ΔP_1 clustering to predict the dynamics of the hillslopes in wet and dry conditions. A possible limitation of a clustering based on a hydrologic process is that the latter may be linked to the conditions of the selected year. Hydrologic responses are by essence nonlinear and may strongly change from year to year. In addition, compared to the intrinsic characteristics of the hillslope (elevation, topographic index, and land cover), which are only variable if long periods of time are considered;

the scale at which hydrologic processes change is much shorter. Therefore, a clustering based on a hydrologic process may be time-dependent. We previously quantified ΔP_1 using an average WY. In this section, we compare the response of each zone to dry and wet conditions. We extend our simulation from the WY 2015 to include the WYs 2016, 2017, and 2018, then we analyze WYs 2017 and 2018. This 4-year simulation covers a relatively wet (2017) and dry (2018) WY. The annual average precipitation in 2017 was ~15% higher than the annual average precipitation in 2015. After this wet WY, the watershed is characterized by a dry climate in 2018, with average precipitation almost 50% below the normal conditions. Figure 10 shows the distributions of hillslope annual average values of precipitation and ET, and the hillslope ΔP_2 associated with the defined ΔP_1 zones and for both the wet WY 2017 and the dry WY 2018. We have selected the key variables describing the hydroclimate (Precipitation), land surface processes (ET), and subsurface hydrodynamics (ΔP_2).

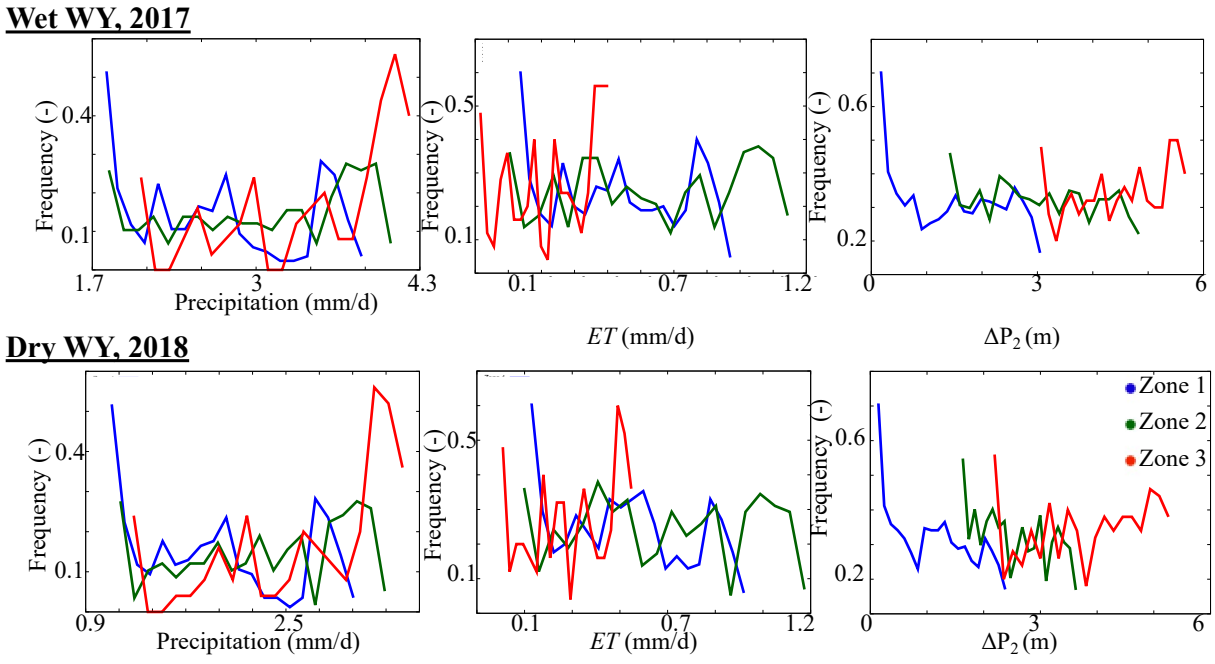

Figure 10: Frequency distributions of hillslope annual average daily rates of precipitation and evapotranspiration (ET), and the hillslope seasonal changes in groundwater levels (ΔP_2) in 2017 (wet WY) and 2018 (dry WY) of the three zones derived from the WY 2015 ΔP_1

At first glance, for both dry and wet years and selected processes, all zones remain distinct. Zone 1 with hillslopes with low ΔP_1 located in low elevation remains with low precipitation, high ET through both wet and dry years. Zone 3 describing hillslopes with high ΔP_1 has the highest precipitation in the area during both the wet and dry years. Hillslopes of zone 2, located in mid-elevation, have most of their hydrologic dynamics in between those of zone 1 and 3 except their ET, which is the highest in the area due to the presence of forest. Our results show that although we defined hillslopes clustering based on a hydrologic process during an average WY, our clustering approach can predict the similarity of the dynamics of these hillslopes in wet and dry conditions. The ΔP_1 clustering is, therefore, robust in predicting similarity in hydrologic responses under both wet and dry conditions.

5. Summary and conclusions

In this study, we use seasonal changes in groundwater levels termed ΔP_1 to identify and categorize similar hillslopes. ΔP_1 is an important variable controlled by many hydrologic processes including land surface processes and hydroclimatic. We defined three zones based on their similarity in ΔP_1. For a test case site in the East River watershed, zone 1 characterizes hillslopes with low ΔP_1; these hillslopes are mostly located in low elevation areas, their main land cover is grassland, and their ET is high because their WTDs are shallow. Zone 3, on the opposite of zone 1 is located in high elevation areas and has high ΔP_1; the hydroclimate leads to high snow

accumulation and low ET. Hillslopes of zone 3 are mostly bare soil. Zone 2 is in-between these two zones, most of the hillslopes of this zone are covered by forests.

We tested the performance of the proposed ΔP_1 clustering by comparing it with other existing clustering approaches based on elevation, land cover, aridity index, a topographic wetting index, and three clustering approaches based on machine learning which uses multiple data layers, including model inputs and outputs. Our results show that the ΔP_1 clustering is robust, as it reasonably identifies and categorizes hillslopes with similar elevation, land cover, hydroclimate characteristics, land surface processes (ET and SWE), and subsurface hydrodynamics (WTD, soil moisture, and ΔP_1). In general, the other clustering approaches are good in identifying similarity in a single characteristic related to the variable determining the clustering. Our work also demonstrates that a clustering using machine learning, either based on top-down (inputs) or bottom-up (outputs) performs well. Nevertheless, these clustering approaches like the ΔP_1, require multiple datasets, each one with its own associated uncertainty. We further demonstrate the robustness of the proposed ΔP_1 clustering by testing its ability to predict hillslope responses to wet and dry hydrologic conditions. The ΔP_1 values are derived from a model and could be a limitation for sites where simulated outputs are unavailable, or the spatio-temporal resolution of groundwater observations are limited. In addition, one of the main limitations of the proposed clustering is that due to the disconnection between land surface processes and structures and the subsurface dynamics in some regions, this clustering approach cannot be used in these conditions.

Future studies could aim to identify similar hillslopes using ΔP_1 and sophisticated machine learning approaches or optimization procedures. Our results are limited to one catchment, which has snow-dominated hydrology. Future studies could expand the comparison shown here to other

watersheds, to include additional clustering approaches, and for different hydroclimate and durations of time (for example, sub-annual or multi-annual clustering).

Data availability

Data supporting the findings of this study are freely available on ESS-DIVE: https://ess-dive.lbl.gov

Author contribution

The authors contribute equally to this work.

Competing interests

The authors declare that they have no conflict of interest.

Acknowledgements

This material is based on work supported as part of the Watershed Function Scientific Focus Area funded by the U.S. Department of Energy, Office of Science, Office of Biological and Environmental Research under Award no. DE-AC02-05CH11231.

Appendix A

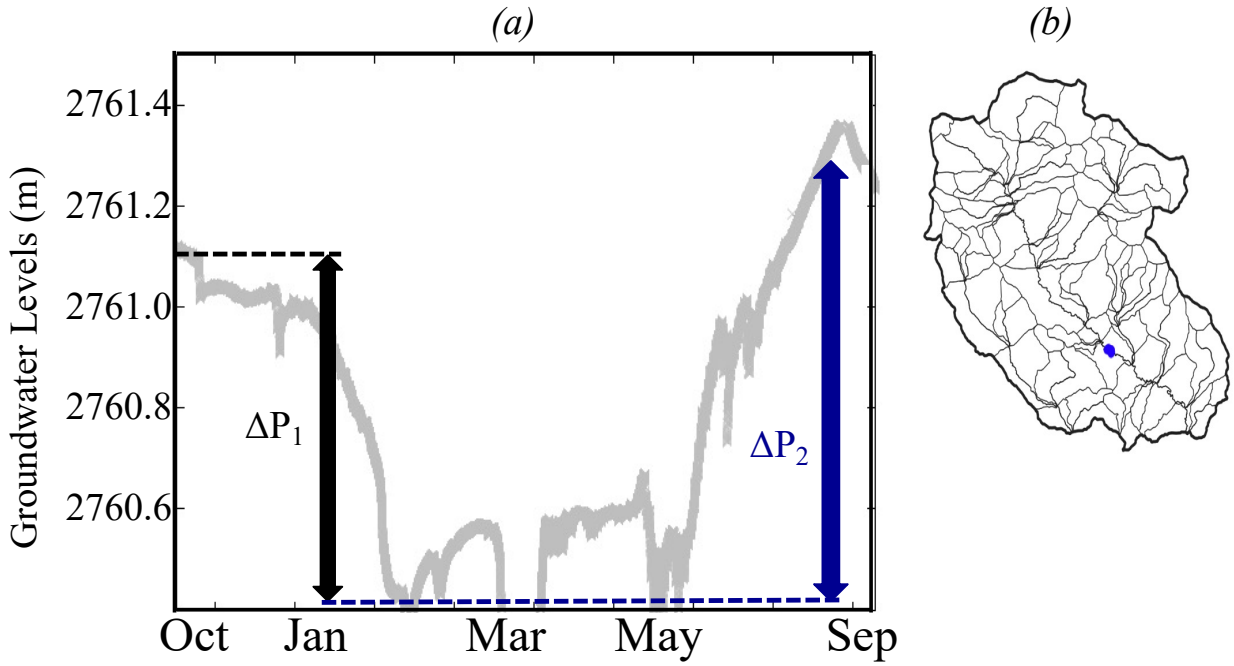

Figure A1: (a) Measured groundwater levels in WY2016 at a station located in blue in (b)

References

Andréassian, V., Lerat, J., Le Moine, N., & Perrin, C. (2012). Neighbors: Nature's own hydrological models. *Journal of Hydrology*, *414–415*, 49–58. https://doi.org/10.1016/j.jhydrol.2011.10.007

Aryal, S. K., O'Loughlin, E. M., & Mein, R. G. (2002). A similarity approach to predict landscape saturation in catchments. *Water Resources Research*, *38*(10), 26-1-26–16. https://doi.org/10.1029/2001WR000864

Berghuijs, W. R., Sivapalan, M., Woods, R. A., & Savenije, H. H. G. (2014). Patterns of similarity of seasonal water balances: A window into streamflow variability over a range of time scales. *Water Resources Research*, *50*(7), 5638–5661. https://doi.org/10.1002/2014WR015692

Berne, A., Uijlenhoet, R., & Troch, P. A. (2005). Similarity analysis of subsurface flow response of hillslopes with complex geometry. *Water Resources Research*, *41*(9). https://doi.org/10.1029/2004WR003629

Beven, K. J. (2000). Uniqueness of place and process representations in hydrological modelling. *Hydrology and Earth System Sciences*, *4*(2), 203–213. https://doi.org/10.5194/hess-4-203-2000

BEVEN, K. J., & KIRKBY, M. J. (1979). A physically based, variable contributing area model of basin hydrology / Un modèle à base physique de zone d'appel variable de l'hydrologie du bassin versant. *Hydrological Sciences Bulletin*, *24*(1), 43–69. https://doi.org/10.1080/02626667909491834

Bormann, H. (2010). Towards a hydrologically motivated soil texture classification. *Geoderma*, *157*(3), 142–153. https://doi.org/10.1016/j.geoderma.2010.04.005

Bosch, J. M., & Hewlett, J. D. (1982). A review of catchment experiments to determine the effect of vegetation changes on water yield and evapotranspiration. *Journal of Hydrology*, *55*(1), 3–23. https://doi.org/10.1016/0022-1694(82)90117-2

Brown, A. E., Zhang, L., McMahon, T. A., Western, A. W., & Vertessy, R. A. (2005). A review of paired catchment studies for determining changes in water yield resulting from alterations in vegetation. *Journal of Hydrology*, *310*(1), 28–61. https://doi.org/10.1016/j.jhydrol.2004.12.010

Brunner, P., & Simmons, C. T. (2012). HydroGeoSphere: A Fully Integrated, Physically Based Hydrological Model. *Groundwater*, *50*(2), 170–176. https://doi.org/10.1111/j.1745-6584.2011.00882.x

Carrillo, G., Troch, P. A., Sivapalan, M., Wagener, T., Harman, C., & Sawicz, K. (2011). Catchment classification: hydrological analysis of catchment behavior through process-based modeling along a climate gradient. *Hydrology and Earth System Sciences*, *15*(11), 3411–3430. https://doi.org/10.5194/hess-15-3411-2011

Carroll, R. W. H., Bearup, L. A., Brown, W., Dong, W., Bill, M., & Willlams, K. H. (2018). Factors controlling seasonal groundwater and solute flux from snow-dominated basins. *Hydrological Processes*, *32*(14), 2187–2202. https://doi.org/10.1002/hyp.13151

CGIAR-CSI. (2019, January 24). Global Aridity Index and Potential Evapotranspiration Climate Database v2. Retrieved August 22, 2020, from https://cgiarcsi.community/2019/01/24/global-aridity-index-and-potential-evapotranspiration-climate-database-v2/

Chadwick, K. D., Brodrick, P. G., Grant, K., Goulden, T., Henderson, A., Falco, N., Wainwright, H., Williams, K. H., Bill, M., Breckheimer, I., Brodie, E. L., Steltzer, H., Rick Williams,

689 C. F., Blonder, B., Chen, J., Dafflon, B., Damerow, J., Hancher, M., Khurram, A., …
690 Maher, K. (2020). Integrating airborne remote sensing and field campaigns for ecology and
691 earth system science. Methods in Ecology and Evolution, 11, 1492– 1508.
692 https://doi.org/10.1111/2041-210x.13463
693 Chaney, N. W., Van Huijgevoort, M. H. J., Shevliakova, E., Malyshev, S., Milly, P. C. D.,
694 Gauthier, P. P. G., & Sulman, B. N. (2018). Harnessing big data to rethink land
695 heterogeneity in Earth system models. *Hydrology and Earth System Sciences*, *22*(6), 3311–
696 3330. https://doi.org/10.5194/hess-22-3311-2018
697 Condon, L. E., Maxwell, R. M., & Gangopadhyay, S. (2013). The impact of subsurface
698 conceptualization on land energy fluxes. *Advances in Water Resources*, *60*, 188–203.
699 https://doi.org/10.1016/j.advwatres.2013.08.001
700 Cosgrove, B. A., Lohmann, D., Mitchell, K. E., Houser, P. R., Wood, E. F., Schaake, J. C., et al.
701 (2003). Real-time and retrospective forcing in the North American Land Data Assimilation
702 System (NLDAS) project. *Journal of Geophysical Research: Atmospheres*, *108*(D22).
703 https://doi.org/10.1029/2002JD003118
704 Dai, Y., Zeng, X., Dickinson, R. E., Baker, I., Bonan, G. B., Bosilovich, M. G., et al. (2003). The
705 Common Land Model. *Bulletin of the American Meteorological Society*, *84*(8), 1013–
706 1024. https://doi.org/10.1175/BAMS-84-8-1013
707 Daly, C., Halbleib, M., Smith, J. I., Gibson, W. P., Doggett, M. K., Taylor, G. H., et al. (2008).
708 Physiographically sensitive mapping of climatological temperature and precipitation
709 across the conterminous United States. *International Journal of Climatology*, *28*(15),
710 2031–2064. https://doi.org/10.1002/joc.1688

Devadoss, J., Falco, N., Dafflon, B., Wu, Y., Franklin, M., Hermes, A., et al. (2020). Remote Sensing-Informed Zonation for Understanding Snow, Plant and Soil Moisture Dynamics within a Mountain Ecosystem. *Remote Sensing*, *12*(17), 2733. https://doi.org/10.3390/rs12172733

Fan, Y., Clark, M., Lawrence, D. M., Swenson, S., Band, L. E., Brantley, S. L., et al. (2019). Hillslope Hydrology in Global Change Research and Earth System Modeling. *Water Resources Research*, *55*(2), 1737–1772. https://doi.org/10.1029/2018WR023903

Fan, Y., Clark, M., Lawrence, D. M., Swenson, S., Band, L. E., Brantley, S. L., Brooks, P. D., Dietrich, W. E., Flores, A., Grant, G., Kirchner, J. W., Mackay, D. S., McDonnell, J. J., Milly, P. C. D., Sullivan, P. L., Tague, C., Ajami, H., Chaney, N., Hartmann, A., Hazenberg, P., McNamara, J., Pelletier, J., Perket, J., Rouholahnejad-Freund, E., Wagener, T., Zeng, X., Beighley, E., Buzan, J., Huang, M., Livneh, B., Mohanty, B. P., Nijssen, B., Safeeq, M., Shen, C., van Verseveld, W., Volk, J., and Yamazaki, D. (2019). Hillslope hydrology in global change research and Earth system modeling, Water Resour. Res., 55, 1737–1772, https://doi.org/10.1029/2018WR023903.

Falco N ; Balde A ; Breckheimer I ; Brodie E ; G. Brodrick P ; Chadwick K D ; Chen J ; Dafflon B ; Henderson A ; Lamb J ; Maher K ; Kueppers L ; Steltzer H ; Wainwright H ; Williams K ; S. Hubbard S (2020): Plant species distribution within the Upper Colorado River Basin estimated by using hyperspectral and LiDAR airborne data. Watershed Function SFA, ESS-DIVE repository. Dataset. doi:10.15485/1602034 accessed via https://data.ess-dive.lbl.gov/datasets/doi:10.15485/1602034 on 2022-03-29

Ferguson, I. M., & Maxwell, R. M. (2010). Role of groundwater in watershed response and land surface feedbacks under climate change. *Water Resources Research*, *46*(10). https://doi.org/10.1029/2009WR008616

Freeze, R. A., & Harlan, R. L. (1969). Blueprint for a physically-based, digitally-simulated hydrologic response model. *Journal of Hydrology*, *9*(3), 237–258. https://doi.org/10.1016/0022-1694(69)90020-1

Foster, L.M., Williams, K.H., Maxwell, R.M., 2020. Resolution matters when modeling climate change in headwaters of the Colorado River. Environ. Res. Lett. https://doi.org/10.1088/1748-9326/aba77f

van Genuchten, M. Th. (1980). A Closed-form Equation for Predicting the Hydraulic Conductivity of Unsaturated Soils1. *Soil Science Society of America Journal*, *44*(5), 892. https://doi.org/10.2136/sssaj1980.03615995004400050002x

Grabs, T., Seibert, J., Bishop, K., & Laudon, H. (2009). Modeling spatial patterns of saturated areas: A comparison of the topographic wetness index and a dynamic distributed model. *Journal of Hydrology*, *373*(1), 15–23. https://doi.org/10.1016/j.jhydrol.2009.03.031

Goulden T ; Hass B ; Brodie E ; Chadwick K D ; Falco N ; Maher K ; Wainwright H ; Williams K (2020): NEON AOP Survey of Upper East River CO Watersheds: LAZ Files, LiDAR Surface Elevation, Terrain Elevation, and Canopy Height Rasters. Watershed Function SFA, ESS-DIVE repository. Dataset. doi:10.15485/1617203 accessed via https://data.ess-dive.lbl.gov/datasets/doi:10.15485/1617203 on 2022-03-29

Harman, C., & Sivapalan, M. (2009). A similarity framework to assess controls on shallow subsurface flow dynamics in hillslopes. *Water Resources Research*, *45*(1). https://doi.org/10.1029/2008WR007067

Hjerdt, K. N., McDonnell, J. J., Seibert, J., & Rodhe, A. (2004). A new topographic index to quantify downslope controls on local drainage. *Water Resources Research*, *40*(5). https://doi.org/10.1029/2004WR003130

Hubbard, S. S., Williams, K. H., Agarwal, D., Banfield, J., Beller, H., Bouskill, N., et al. (2018). The East River, Colorado, Watershed: A Mountainous Community Testbed for Improving Predictive Understanding of Multiscale Hydrological–Biogeochemical Dynamics. *Vadose Zone Journal*, *17*(1), 180061. https://doi.org/10.2136/vzj2018.03.0061

IGBP. (2018). Global plant database published - IGBP [text]. Retrieved October 17, 2018, from http://www.igbp.net/news/news/news/globalplantdatabasepublished.5.1b8ae20512db692f2a6800014762.html

Jefferson, J. L., Gilbert, J. M., Constantine, P. G., & Maxwell, R. M. (2015). Active subspaces for sensitivity analysis and dimension reduction of an integrated hydrologic model. *Computers & Geosciences*, *83*, 127–138. https://doi.org/10.1016/j.cageo.2015.07.001

Kassambara, A. (2017). *Practical guide to cluster analysis in R: Unsupervised machine learning* (Vol. 1). Sthda.

Loritz, R., Kleidon, A., Jackisch, C., Westhoff, M., Ehret, U., Gupta, H., & Zehe, E. (2019). A topographic index explaining hydrological similarity by accounting for the joint controls of runoff formation. *Hydrology and Earth System Sciences*, *23*(9), 3807–3821. https://doi.org/10.5194/hess-23-3807-2019

Lyon, S. W., & Troch, P. A. (2007). Hillslope subsurface flow similarity: Real-world tests of the hillslope Péclet number. *Water Resources Research*, *43*(7). https://doi.org/10.1029/2006WR005323

Lyon, Steve W., & Troch, P. A. (2010). Development and application of a catchment similarity index for subsurface flow. *Water Resources Research*, *46*(3). https://doi.org/10.1029/2009WR008500

Maina, F. Z., & Siirila-Woodburn, E. R. (2020). The Role of Subsurface Flow on Evapotranspiration: A Global Sensitivity Analysis. *Water Resources Research*, *56*(7), e2019WR026612. https://doi.org/10.1029/2019WR026612

Maina, Fadji Z., Siirila-Woodburn, E. R., & Dennedy-Frank, P. J. (2022) Assessing the impacts of hydrodynamic parameter uncertainties on simulated evapotranspiration in a mountainous watershed. *Journal of Hydrology* 608. https://doi.org/10.1016/j.jhydrol.2022.127620.

Maxwell, R. M. (2013). A terrain-following grid transform and preconditioner for parallel, large-scale, integrated hydrologic modeling. *Advances in Water Resources*, *53*, 109–117. https://doi.org/10.1016/j.advwatres.2012.10.001

Maxwell, R. M., & Miller, N. L. (2005). Development of a Coupled Land Surface and Groundwater Model. *Journal of Hydrometeorology*, *6*(3), 233–247. https://doi.org/10.1175/JHM422.1

McDonnell, J. J., & Woods, R. (2004). On the need for catchment classification. *Journal of Hydrology*, *299*, 2–3. https://doi.org/10.1016/j.jhydrol.2004.09.003

Noël, P., Rousseau, A. N., Paniconi, C., & Nadeau, D. F. (2014). Algorithm for Delineating and Extracting Hillslopes and Hillslope Width Functions from Gridded Elevation Data. *Journal of Hydrologic Engineering*, *19*(2), 366–374. https://doi.org/10.1061/(ASCE)HE.1943-5584.0000783

798 Oudin, L., Kay, A., Andréassian, V., & Perrin, C. (2010). Are seemingly physically similar
799 catchments truly hydrologically similar? *Water Resources Research*, *46*(11).
800 https://doi.org/10.1029/2009WR008887
801 Pribulick, C. E., Foster, L. M., Bearup, L. A., Navarre-Sitchler, A. K., Williams, K. H., Carroll, R.
802 W. H., & Maxwell, R. M. (2016). Contrasting the hydrologic response due to land cover
803 and climate change in a mountain headwaters system. *Ecohydrology*, *9*(8), 1431–1438.
804 https://doi.org/10.1002/eco.1779
805 Rahman, M., Sulis, M., & Kollet, S. J. (2016). Evaluating the dual-boundary forcing concept in
806 subsurface–land surface interactions of the hydrological cycle. *Hydrological Processes*,
807 *30*(10), 1563–1573. https://doi.org/10.1002/hyp.10702
808 Richards, L. A. (1931). Capillary conduction of liquids through porous medium. *Journal of*
809 *Applied Physics*, *1*(5), 318–333. https://doi.org/10.1063/1.1745010
810 Ryken, A., Bearup, L. A., Jefferson, J. L., Constantine, P., & Maxwell, R. M. (2020). Sensitivity
811 and model reduction of simulated snow processes: Contrasting observational and
812 parameter uncertainty to improve prediction. *Advances in Water Resources*, *135*, 103473.
813 https://doi.org/10.1016/j.advwatres.2019.103473
814 Sawicz, K., Wagener, T., Sivapalan, M., Troch, P. A., & Carrillo, G. (2011). Catchment
815 classification: empirical analysis of hydrologic similarity based on catchment function in
816 the eastern USA. *Hydrology and Earth System Sciences*, *15*(9), 2895–2911.
817 https://doi.org/10.5194/hess-15-2895-2011
818 Schwanghart, W., & Scherler, D. (2014). Short Communication: TopoToolbox 2 – MATLAB-
819 based software for topographic analysis and modeling in Earth surface sciences. *Earth*
820 *Surface Dynamics*, *2*(1), 1–7. https://doi.org/10.5194/esurf-2-1-2014

821 SIVAPALAN, M., TAKEUCHI, K., FRANKS, S. W., GUPTA, V. K., KARAMBIRI, H.,
822 LAKSHMI, V., et al. (2003). IAHS Decade on Predictions in Ungauged Basins (PUB),
823 2003–2012: Shaping an exciting future for the hydrological sciences. *Hydrological*
824 *Sciences Journal*, *48*(6), 857–880. https://doi.org/10.1623/hysj.48.6.857.51421
825 Wagener, T., Sivapalan, M., Troch, P., & Woods, R. (2007). Catchment Classification and
826 Hydrologic Similarity. *Geography Compass*, *1*(4), 901–931.
827 https://doi.org/10.1111/j.1749-8198.2007.00039.x
828 Wainwright, H. M., Uhlemann, S., Franklin, M., Falco, N., Bouskill, N. J., Newcomer, M.,
829 Dafflon, B., Woodburn, E., Minsley, B. J., Williams, K. H., and Hubbard, S. S. (2022).
830 Watershed zonation approach for tractably quantifying above-and-belowground watershed
831 heterogeneity and functions, *Hydrol. Earth Syst. Sci., https://doi.org/10.5194/hess-2021-*
832 *228*.
833